Methods

MSP data

Table 1 gives the positions and number of MSP profiles forming the station averages, and references to the expeditions that collected them. We used data from below the seasonal thermocline, where the GM model should apply, and where the mean shear was weak. Owing to the strong mean shear in the main thermocline near and on the Equator during Tropic Heat 2, only data from the lower thermocline were used. COARE3 data on the Equator were used between 400–640 m and 640–890 m because we found no significant mean shear. Mean shear was weak near the centre of the Straits of Florida at stations 5 and 6, which were averaged between 205–305, 305–405 and 405–505 m. The C-SALT profiles were taken just outside the thermohaline staircase.

Dissipation rates

Shear spectra of airfoil records were calculated over 2-m intervals, and integrated to estimate local dissipation rates along each profile. Histograms of each depth interval and station were examined to estimate the noise level for the ensemble. The noise levels varied from 5×10^{-11} to 8×10^{-11} W kg^{-1}, probably owing to differing noise characteristics of the airfoils. Estimates at or below the noise level were set to zero on the assumption that no mixing occurred. This was consistent with the lack of identifiable density overturns in these intervals, but we could not always be certain owing to the half-metre vertical resolution attainable with the Sea-Bird temperature and salinity records. Averages and confidence limits were computed using bootstrap[18] techniques. Zeroing noisy ε values made little difference in most averages, but it reduced the COARE3 deep average at 3° N by one-half, and the Tropic Heat 2 data at 11.5° N by two-thirds. Using the unconditional averages would put the former within and the latter above the plotted bounds of 0.5 and 2 times the prediction.

Predicting the dissipation rate

Dissipation rates were predicted by evaluating the first part of equation (1) expressed as:

$$\varepsilon_{30^\circ} = 6.73\times10^{-10}\left(\frac{N}{N_0}\right)^2\left(\frac{0.1}{k_c}\right)^2\left(\frac{1+1/R}{4/3}\right)\left(\frac{2}{R-1}\right)^{1/2} \quad (4)$$

where ε_{30° is in units of W kg^{-1}. This equation of is a slight modification of the formulation of ref. 5. N_0 is the GM model reference stratification 5.24×10^{-3} s^{-1}, k_c is the high-wavenumber cut-off of the internal wave shear spectrum, and R is a dimensionless ratio defined below. To accommodate varied spectral shapes, the shear spectrum is integrated until the variance reaches $0.661\,N^2$, that is, $\int_{k_0}^{k_c}\Phi_{\text{shear}}^{\text{observed}}(m)\,dm = 0.661N^2$. The upper limit k_c is taken to be the high-wavenumber cut-off, and k_0 is the reciprocal of the length of record being analysed. The reference variance is obtained by integrating the white GM shear spectrum to its cut-off at 0.1 cycles per metre, that is $\int_{0.005}^{0.1}\Phi_{\text{shear}}^{\text{GM}}(m)\,dm = 0.661N^2$. Consequently, at vertical wavenumbers less than k_c, the ratio of the average spectral levels is $\Phi_{\text{shear}}^{\text{observed}}/\Phi_{\text{shear}}^{GM} = 0.1/k_c$. The second term in equation (4) is the square of this ratio, and is plotted in Fig. 3. R is the average ratio of the shear variance normalized by N^2 to the strain variance, both integrated to k_c. Dependent on R, the third and fourth terms in equation (4) are corrections for variations in the ratio of total energy to horizontal kinetic energy and in the dominant frequency content, both relative to the GM model.

The latitude dependence, equation (2), is the analytic form in the theoretical model[3] and has not been previously tested. As noted earlier, it arises because the rate at which the evolving waves are Doppler shifted depends on the ratio between their vertical and horizontal length scales. This is expressed by $\frac{l_{\text{vert}}}{l_{\text{horiz}}} = \left\langle\frac{\omega^2-f^2}{N^2-\omega^2}\right\rangle_{\text{GM}}^{1/2} = \frac{f}{N}\cosh^{-1}\left(\frac{N}{f}\right)$, where averaging is across the internal wave frequency range, $f \leq \omega \leq N$, and is weighted by the frequency content of the GM wave field. Comparison to the GM reference at 30° leads to equation (2). Because N/f is a large number, $\cosh^{-1}(N/f) \approx \ln(2N/f)$.

Received 19 July 2002; accepted 14 February 2003; doi:10.1038/nature01507.

1. National Science Foundation *Ocean Sciences at the New Millennium* (NSF, Washington DC, 2001).
2. McComas, C. H. & Muller, P. The dynamic balance of internal waves. *J. Phys. Oceanogr.* **11,** 970–986 (1981).
3. Henyey, F. S., Wright, J. & Flatte, S. M. Energy and action flow through the internal wave field: An eikonal approach. *J. Geophys. Res.* **91,** 8487–8495 (1986).
4. Gregg, M. C. Scaling turbulent dissipation in the thermocline. *J. Geophys. Res.* **94,** 9686–9698 (1989).
5. Polzin, K., Toole, J. M. & Schmitt, R. W. Finescale parameterization of turbulent dissipation. *J. Phys. Oceanogr.* **25,** 306–328 (1995).
6. Garrett, C. J. R. & Munk, W. H. Space-time scales of internal waves: A progress report. *J. Geophys. Res.* **80,** 291–297 (1975).
7. Munk, W. H. in *Evolution of Physical Oceanography* (eds Warren, B. A. & Wunsch, C.) 264–291 (MIT Press, Cambridge, Massachusetts, 1981).
8. Sun, H. & Kunze, E. Internal wave-wave interactions. Part II: Spectral energy transfer and turbulence production. *J. Phys. Oceanogr.* **29,** 2905–2919 (1999).
9. Henyey, H. F. in *Dynamics of Internal Gravity Waves in the Ocean: Proceedings, 'Aha Huliko'a Hawaiian Winter Workshop* (eds Muller, P. & Henderson, D.) 233–236 (Spec. publ. SOEST, Univ. Hawaii, 1991).
10. Winkel, D. P., Gregg, M. C. & Sanford, T. B. Resolving oceanic shear and velocity with the Multi-Scale Profiler. *J. Atmos. Ocean. Technol.* **13,** 1046–1072 (1996).
11. Osborn, T. R. Estimates of the local rate of vertical diffusion from dissipation measurements. *J. Phys. Oceanogr.* **20,** 83–89 (1980).
12. Davis, R. E. Diapycnal mixing in the ocean: The Osborn-Cox model. *J. Phys. Oceanogr.* **24,** 2560–2576 (1994).
13. Ledwell, J. R., Watson, A. J. & Law, C. S. Evidence for slow mixing across the pycnocline from an open-ocean tracer release experiment. *Nature* **364,** 701–703 (1993).
14. Toole, J. M., Polzin, K. L. & Schmitt, R. W. Estimates of diapycnal mixing in the abyssal ocean. *Science* **264,** 1120–1123 (1994).
15. Ledwell, J. R. *et al.* Evidence for enhanced mixing over rough topography in the abyssal ocean. *Nature* **403,** 179–182 (2000).
16. Gregg, M. C. Variations in the intensity of small-scale mixing in the main thermocline. *J. Phys. Oceanogr.* **7,** 436–454 (1977).
17. Nagasawa, M., Niwa, Y. & Hibiya, T. Spatial and temporal distribution of wind-induced internal wave energy available for deep water mixing in the North Pacific. *J. Geophys. Res.* **105,** 13933–13943 (2000).
18. Efron, G. & Gong, G. A leisurely look at the bootstrap, the jackknife, and cross-validation. *Am. Stat.* **37,** 36–48 (1983).
19. Gregg, M. C., Winkel, D. P., Sanford, T. B. & Peters, H. Turbulence produced by internal waves in the oceanic thermocline at mid and low latitudes. *Dynam. Atmos. Oceans* **24,** 1–14 (1996).
20. Peters, H., Gregg, M. C. & Sanford, T. B. Equatorial and off-equatorial shear variability at 140° W. *J. Geophys. Res.* **96,** 16913–16928 (1991).
21. Schmitt, R. W., Perkins, H., Boyd, J. D. & Stalcup, M. C. C-SALT: an investigation of the thermohaline staircase in the western tropical North Atlantic. *Deep-Sea Res.* **34,** 1655–1665 (1987).
22. Gregg, M. C. & Sanford, T. B. Shear and turbulence in thermohaline staircases. *Deep-Sea Res.* **34,** 1689–1696 (1987).
23. Winkel, D. P., Gregg, M. C. & Sanford, T. B. Patterns of shear and turbulence across the Florida Current. *J. Phys. Oceanogr.* **32,** 3269–3285 (2002).
24. Gregg, M. C. & Sanford, T. B. The dependence of turbulent dissipation on stratification in a diffusively stable thermocline. *J. Geophys. Res.* **93,** 12381–12392 (1988).

Acknowledgements The Office of Naval Research and the National Science Foundation funded our instrumentation and data collection. A SECNAV/CNO fellowship in oceanography supported M.C.G. during the analysis and writing of this letter.

Competing interests statement The authors declare that they have no competing financial interests.

Correspondence and requests for materials should be addressed to M.C.G. (e-mail: gregg@apl.washington.edu).

Cannibalism in the Madagascan dinosaur *Majungatholus atopus*

Raymond R. Rogers*, David W. Krause† & Kristina Curry Rogers‡

** Geology Department, Macalester College, 1600 Grand Avenue, St Paul, Minnesota 55105, USA*
† Department of Anatomical Sciences, Stony Brook University, Stony Brook, New York 11794, USA
‡ Department of Paleontology, Science Museum of Minnesota, 120 West Kellogg Boulevard, St Paul, Minnesota 55102, USA

Many lines of evidence have been brought to bear on the question of theropod feeding ecology, including functional and physiological considerations, morphological constraints, taphonomic associations, and telling—although rare—indications of direct ingestion[1–7]. Tooth marks of theropods, although rarely described and generally left unassigned to a particular taxon, can provide unique clues into predator–prey interaction[8], and can also yield insights into the extent of carcass utilization[9,10]. Here we describe a sample of tooth-marked dinosaur bone recovered from three well-documented localities in the Upper Cretaceous Maevarano Formation of Madagascar that provides insights into the feeding ecology of the abelisaurid theropod *Majungatholus atopus*[11]. Intensely tooth-marked elements from multiple individuals show that *Majungatholus* defleshed dinosaur carcasses. Furthermore, *Majungatholus* clearly fed upon the remains of not only sauropods, but also conspecifics, and thus was a cannibal. Cannibalism is a common ecological strategy among extant carnivores, but until now the evidence in relation to carnivorous dinosaurs has been sparse and anecdotal.

Majungatholus atopus inhabited the plains of northwestern Madagascar during the Late Cretaceous. Its bones and teeth are found throughout the Maevarano Formation (Campanian–Maastrichtian), but are most abundant within the channel-belt deposits of the Anembalemba Member[12]. Here, the remains of *Majungatholus* are commonly found in association with those of

other vertebrate taxa in spectacular 'bonebeds'[13]. For example, quarry MAD96-01 yielded a nearly complete skull, lower jaws, and associated postcranial elements of a single *Majungatholus* individual (Field Museum of Natural History FMNH PR2100)[11], as well as the remains of fish, turtles, crocodyliforms, sauropods, birds and mammals. At least 12 postcranial elements of *Majungatholus* preserved at this locality (including five chevrons, three neural arches, two transverse processes, one neural spine and one rib) exhibit tooth marks (Fig. 1). Three chevrons, one transverse process and the neural spine exhibit parallel sets of tooth marks. Two chevrons from this site exhibit drag marks from denticles on the tooth carinae.

Another bonebed in the Anembalemba Member, quarry MAD96-21, yielded disarticulated skull elements, the left ilium, and most of the precaudal axial column of a subadult *Majungatholus* (University of Antananarivo UA 8678) in association with rare frog, turtle, crocodyliform and sauropod elements. The bones of this subadult individual are again scored by numerous conspicuous tooth marks, and at least nine *Majungatholus* elements recovered from this site exhibit evidence of feeding by a fairly large and persistent vertebrate carnivore. The most frequently marked elements are ribs, although at least two neural arches from the site also exhibit tooth marks. Two ribs in the sample exhibit bite marks on both superficial and deep aspects of the element. Multiple sets of denticle drag marks accompany tooth marks on one rib (Fig. 2a, b).

Denticle drag marks on two specimens (FMNH PR2100 (chevron, field number 96313-31D, quarry MAD96-01) and UA 8678 (rib, field number 96300-C, quarry MAD96-21): Figs 1c and 2a, b) were measured, and average 2.1 denticles mm^{-1}. Ten *Majungatholus* crowns from quarry MAD93-18 were selected at random for comparison. On average, the ten teeth are characterized by 2 denticles mm^{-1}, with a range of 1.9–2.5 denticles mm^{-1}. Measurements taken from the modified bones and the *Majungatholus* teeth are definitely comparable. The set of parallel tooth marks on specimen 96313-31D (Fig. 1c) was also measured to approximate intertooth spacing in the perpetrator's jaw. Tooth marks on this element are spaced 1.0–1.7 cm apart. Comparable intertooth spacing, with values ranging from 1.3 to 2.3 cm, characterizes the tooth-bearing elements of the *Majungatholus* specimen (FMNH PR2100) collected from MAD96-01: the slightly lower spacing values on the chevron are easily explained by the angle at which the tooth row intersected the bone. It should also be noted that *Majungatholus atopus* can exhibit an even pattern of tooth eruption, as exemplified by the right dentary of FMNH PR2100 (Fig. 2c). An even pattern of tooth eruption would be needed to generate the set of tooth marks on specimen 96313-31D, and several other bones in the sample. These observations (with the caveats that tooth eruption varies among individuals, and intertooth spacing varies with ontogeny), in combination with the denticle drag patterns described above, make a compelling case for *Majungatholus* feeding on *Majungatholus* carrion at both MAD96-01 and MAD96-21.

Additional evidence of feeding behaviour can be found in collections from quarry MAD93-18, which include the remains of the small theropod *Masiakasaurus knopfleri*[14], juvenile and adult specimens of the sauropod *Rapetosaurus krausei*[15], along with fish, turtles, snakes, crocodyliforms, birds, mammals, and the bones and

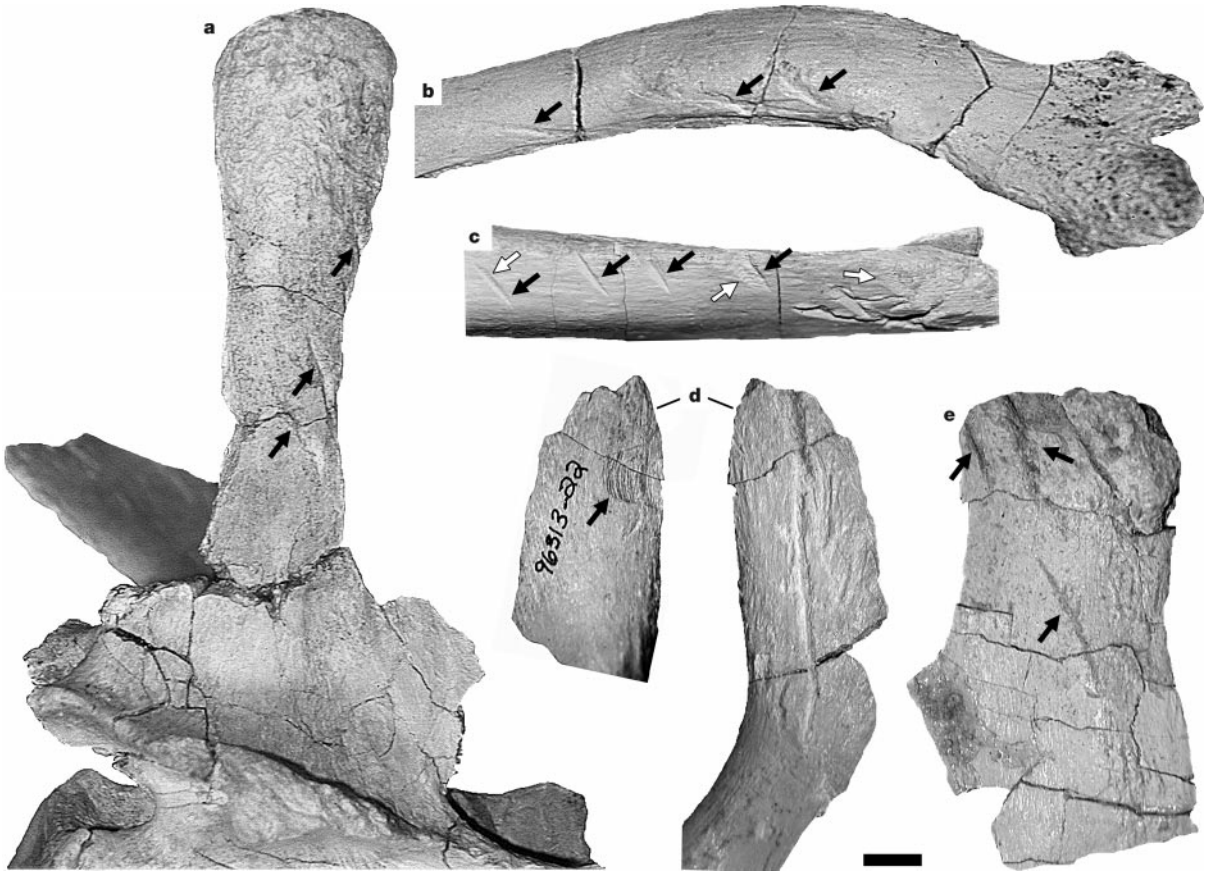

Figure 1 Representative sample of tooth-marked *Majungatholus atopus* bones (FMNH PR2100) from quarry MAD96-01. **a**, Caudal vertebra (field number 96313-14) with set of parallel tooth marks (arrows) on anterior edge of neural spine. **b**, Chevron (field number 96212-44C) with set of parallel tooth marks (arrows) on posterior margin. **c**, Chevron (field number 96313-31D) with set of four parallel tooth marks (black arrows), deep tooth gouges, and denticle drag marks (white arrows). **d**, Chevron (field number 96313-22) gouged with denticle drag marks (right-lateral view, arrow) and deep tooth drag (left-lateral view). **e**, Transverse process (field number 96313-31) with multiple tooth marks (arrows). Scale bar, 1 cm.

teeth of *Majungatholus*. A large *Rapetosaurus* pubis from this locality exhibits a conspicuous concentration of sub-parallel furrows along the element's distal margin (Fig. 3). The size, shallow U-shaped morphology, and subparallel configuration of the traces are consistent with infliction by the premaxillary teeth of *Majungatholus*, which may have been processing the end of this element in an attempt to procure marrow and/or spongy bone. At least two additional bones from this site, a theropod rib and a sauropod chevron, also exhibit tooth marks.

The only other theropod known from the Maevarano Formation is *Masiakasaurus knopfleri*, whose small size precludes it from generating the tooth marks in question (Fig. 4). It is also possible to rule out the contemporaneous large crocodyliforms *Trematochampsa*[16] and *Mahajangasuchus*[17], because their robust, conical teeth were too blunt, too irregularly spaced, too variable in height, too variable in orientation (especially *Mahajangasuchus*, whose anterior teeth were procumbent), and too variably positioned (buccolingually) relative to the longitudinal axis of the jaw (especially *Trematochampsa*) to inflict the sets of narrow U-shaped grooves documented on the bones of *Majungatholus* (Figs 1 and 4). Of the medium- to large-bodied carnivores in the Maevarano Formation's vertebrate assemblage, only *Majungatholus atopus* possessed dentition capable of inflicting the suite of tooth marks documented in quarries MAD96-01, MAD96-21 and MAD93-18.

Data from three separate bonebeds indicate that *Majungatholus atopus* regularly defleshed dinosaur carcasses. The main focus seems to have been along the axial column, although appendicular elements such as the sauropod pubis in quarry MAD93-18 also show evidence of concerted effort. There is also indication that *Majungatholus atopus* fed upon the remains of its own dead, and thus supplemented its diet via cannibalism. The evidence comes in the form of at least 21 tooth-marked elements derived from two *Majungatholus* individuals (FMNH PR2100 and UA 8678) preserved in two separate localities (quarries MAD96-01 and MAD96-21). Whether *Majungatholus* killed both individuals and thus practiced intraspecific predation, or opportunistically scavenged their remains, is unknown.

Cannibalism as an ecological strategy is not uncommon among extant animals. At least 14 species of mammalian carnivores kill and eat members of their own species, and numerous reptilian and avian taxa also practice cannibalism[18–22]. In contrast, the evidence for cannibalism among dinosaurs is meagre. The most celebrated example of a dinosaur cannibal is the Triassic theropod *Coelophysis*

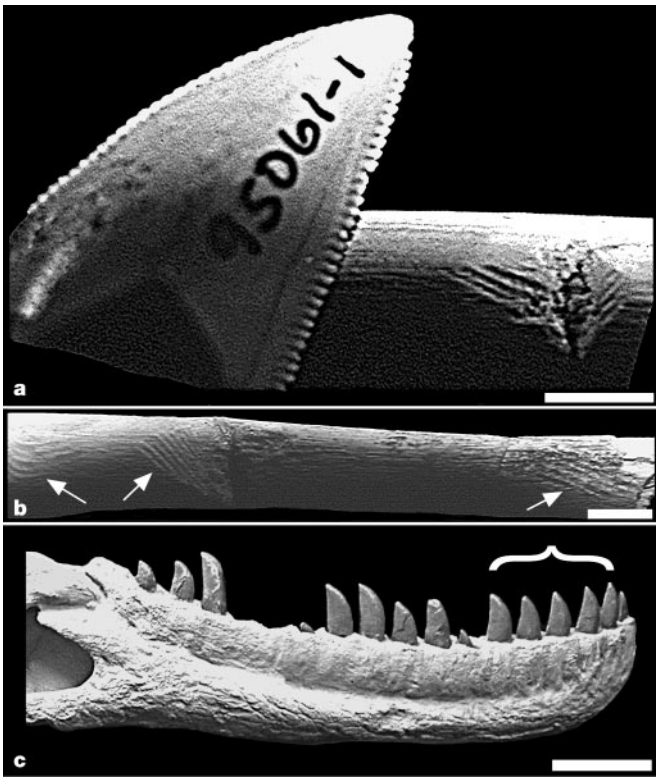

Figure 2 Physical evidence linking *Majungatholus atopus* to the tooth marks. **a**, **b**, *Majungatholus atopus* rib (UA 8678, field number 96300-C) from quarry MAD96-21 that exhibits multiple sets of denticle drag marks (both views are different regions of the same rib). The chisel-like morphology and spacing of the denticles on the *Majungatholus* tooth shown in **a** are comparable to the denticle patterns on modified bones. Teeth of *Majungatholus* occasionally exhibit damaged and/or worn denticles, which presumably reflects contact with bone. Scale bars, 5 mm. **c**, The right dentary of *Majungatholus atopus* (FMNH PR2100) collected from MAD96-01 exemplifies the even pattern of tooth eruption (beneath bracket) required to generate the parallel sets of tooth marks documented on several bones in the sample. The intertooth spacing of *Majungatholus* is also consistent with the pattern of tooth marks. Scale bar, 5 cm.

Figure 3 *Rapetosaurus krausei* pubis (FMNH PR2255) from quarry MAD93-18 with evidence of peripheral feeding along the element's distal margin. The size, shallow U-shaped morphology, and subparallel configuration of the furrows are consistent with infliction by premaxillary teeth of *Majungatholus atopus*. These traces are morphologically distinct from trample marks, which tend to be much smaller, and to occur in sets of parallel striations. Scale bar, 1 cm.

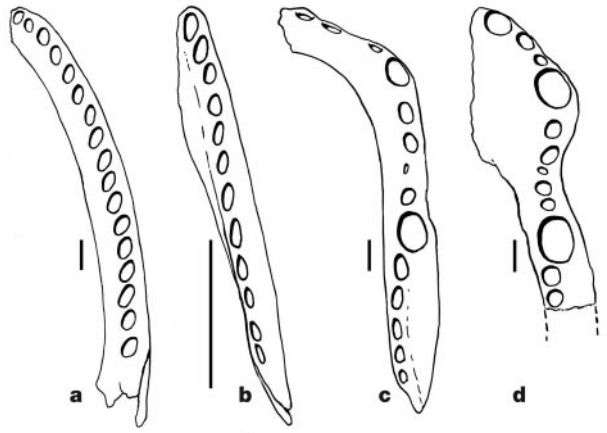

Figure 4 Occlusal views of right dentaries of selected carnivorous taxa in the Maevarano Formation. Taxa shown include *Majungatholus atopus* (**a**), *Masiakasaurus knopfleri* (**b**), *Mahajangasuchus insignis* (**c**) and *Trematochampsa oblita* (**d**). All scale bars, 2 cm. The theropod *Masiakasaurus* was too small to inflict the suite of tooth marks in question. The crocodyliforms *Mahajangasuchus* and *Trematochampsa* both possessed dentition that effectively rules them out as well: their conical teeth were too blunt, too irregularly spaced, too variable in height, and too variable in orientation to inflict the tooth marks on the bones of *Majungatholus atopus* and *Rapetosaurus krausei*.

bauri[23,24], although a recent reappraisal of the evidence suggests that claims of cannibalistic feeding by *Coelophysis* may be unsubstantiated. Juvenile *Coelophysis* bones traditionally interpreted as an ingested meal may lie stratigraphically at least partially below the rib cage of the proposed cannibal (as opposed to within), and the volume of the purportedly ingested material may exceed reasonable estimates of stomach capacity[25]. Cannibalism has also been tentatively proposed for Late Cretaceous tyrannosaurids on the basis of the occurrence of tooth marks on tyrannosaurid bone. However, multiple tyrannosaurid taxa with morphologically indistinguishable teeth occur in the same unit that yields the tooth-marked bones, so the evidence is equivocal[8]. Other claims of dinosaur cannibalism are largely anecdotal[26]. Thus, *Majungatholus atopus* at the very least joins *Coelophysis bauri* as a dinosaur cannibal, and (on present evidence) may in fact be the only theropod dinosaur with demonstrable cannibalistic tendencies. □

Received 14 November 2002; accepted 17 February 2003; doi:10.1038/nature01532.

1. Chin, K., Tokaryk, T. T., Erickson, G. M. & Calk, L. C. A king-sized theropod coprolite. *Nature* **393,** 680–682 (1998).
2. Erickson, G. M. *et al.* Bite-force estimation for *Tyrannosaurus rex* from tooth-marked bones. *Nature* **382,** 706–708 (1996).
3. Rayfield, E. J. *et al.* Cranial design and function in a large theropod dinosaur. *Nature* **409,** 1033–1037 (2001).
4. Farlow, J. O. A consideration of the trophic dynamics of a Late Cretaceous large-dinosaur community (Oldman Formation). *Ecology* **57,** 841–857 (1976).
5. Farlow, J. O., Brinkman, D. L., Abler, W. L. & Currie, P. J. Size, shape and serration density of theropod dinosaur lateral teeth. *Mod. Geol.* **16,** 161–198 (1991).
6. Maxwell, W. D. & Ostrom, J. H. Taphonomy and paleobiological implications of *Tenontosaurus-Deinonychus* associations. *J. Vert. Paleontol.* **15,** 707–712 (1995).
7. Varricchio, D. J. Gut contents from a Cretaceous tyrannosaurid: implications for theropod digestive tracts. *J. Paleontol.* **75,** 401–406 (2001).
8. Jacobsen, A. R. Feeding behaviour of carnivorous dinosaurs as determined by tooth marks on dinosaur bones. *Hist. Biol.* **13,** 17–26 (1998).
9. Fiorillo, A. R. Prey bone utilization by predatory dinosaurs. *Palaeogeogr. Palaeoclimatol. Palaeoecol.* **88,** 157–166 (1991).
10. Hunt, A. P., Meyer, C. A., Lockley, M. G. & Lucas, S. G. Archaeology, toothmarks and sauropod dinosaur taphonomy. *Gaia* **10,** 225–231 (1994).
11. Sampson, S. D. *et al.* Predatory dinosaur remains from Madagascar: Implications for the Cretaceous biogeography of Gondwana. *Science* **280,** 1048–1051 (1998).
12. Rogers, R. R., Hartman, J. H. & Krause, D. W. Stratigraphic analysis of Upper Cretaceous rocks in the Mahajanga Basin, Madagascar: Implications for ancient and modern faunas. *J. Geol.* **108,** 275–301 (2000).
13. Krause, D. W. *et al.* The Late Cretaceous vertebrate fauna of Madagascar: Implications for Gondwanan paleobiogeography. *GSA Today* **9,** 1–7 (1999).
14. Carrano, M. T., Sampson, S. D. & Forster, C. A. The osteology of *Masiakasaurus knopfleri*, a small abelisauroid (Dinosauria: Theropoda) from the Late Cretaceous of Madagascar. *J. Vert. Paleontol.* **22,** 510–534 (2002).
15. Curry Rogers, K. A. & Forster, C. A. The last of the dinosaur titans: a new sauropod from Madagascar. *Nature* **412,** 530–534 (2001).
16. Buffetaut, E. & Taquet, P. Un nouveau Crocodilien mésosuchien dans le Campanien de Madagascar: *Trematochampsa oblita*, n. sp. *Bull. Soc. Géol. Fr.* **21,** 183–188 (1979).
17. Buckley, G. A. & Brochu, C. A. in *Cretaceous Fossil Vertebrates* (ed. Unwin, D.) 149–175 (Palaeontological Assoc., London, 1999).
18. Bertram, B. Social factors influencing reproduction in wild lions. *J. Zool.* **177,** 463–482 (1975).
19. Polis, G. A. The evolution and dynamics of intraspecific predation. *Annu. Rev. Ecol. Syst.* **12,** 225–251 (1981).
20. Auffenberg, W. *The Behavioral Ecology of the Komodo Monitor* 406 (Univ. Press of Florida, Gainesville, 1981).
21. Fox, L. R. Cannibalism in natural populations. *Annu. Rev. Ecol. Syst.* **6,** 87–106 (1975).
22. Polis, G. A., Myers, C. A. & Hess, W. P. A survey of intraspecific predation within the class Mammalia. *Mammal Rev.* **14,** 187–198 (1984).
23. Colbert, E. H. The Triassic dinosaur *Coelophysis*. *Mus. North. Arizona Bull. Ser.* **57,** 1–160 (1989).
24. Colbert, E. H. *The Little Dinosaurs of Ghost Ranch* 250 (Columbia Univ. Press, New York, 1995).
25. Gay, R. J. The myth of cannibalism in *Coelophysis bauri*. *J. Vert. Paleontol.* **22,** 57A (2002).
26. Cooper, M. R. The prosauropod dinosaur *Massospondylus carinatus* Owen from Zimbabwe: Its biology, mode of life, and phylogenetic significance. *Occ. Pap. Nat. Mus. Rhodesia B* **6,** 689–840 (1981).

Acknowledgements We are grateful to the villagers of Berivotra, the staff of the Institute for the Conservation of Tropical Environments, and the faculty of the University of Antananarivo for logistical support, and all field crew members of the Mahajanga Basin Project for their dedicated efforts. We thank L. Betti-Nash for providing artwork for Fig. 4, and K. Chin, G. Erickson, J. Holstein, B. Koralesky, P. O'Connor, S. Sampson, W. Simpson and J. Thole for comments and discussions. This work was supported by NSF, National Geographic Society and Macalester College.

Competing interests statement The authors declare that they have no competing financial interests.

Correspondence and requests for materials should be addressed to R.R.R. (e-mail: rogers@macalester.edu).

Conservation of total synaptic weight through balanced synaptic depression and potentiation

Sébastien Royer & Denis Paré

Center for Molecular & Behavioral Neuroscience, Rutgers State University, 197 University Avenue, Newark, New Jersey 07102, USA

Memory is believed to depend on activity-dependent changes in the strength of synapses[1]. In part, this view is based on evidence that the efficacy of synapses can be enhanced or depressed depending on the timing of pre- and postsynaptic activity[2–5]. However, when such plastic synapses are incorporated into neural network models, stability problems may develop because the potentiation or depression of synapses increases the likelihood that they will be further strengthened or weakened[6]. Here we report biological evidence for a homeostatic mechanism that reconciles the apparently opposite requirements of plasticity and stability. We show that, in intercalated neurons of the amygdala, activity-dependent potentiation or depression of particular glutamatergic inputs leads to opposite changes in the strength of inputs ending at other dendritic sites. As a result, little change in total synaptic weight occurs, even though the relative strength of inputs is modified. Furthermore, hetero- but not homosynaptic alterations are blocked by intracellular dialysis of drugs that prevent Ca^{2+} release from intracellular stores. Thus, in intercalated neurons at least, inverse heterosynaptic plasticity tends to compensate for homosynaptic long-term potentiation and depression, thus stabilizing total synaptic weight.

To control runaway synapses, many neural network models use normalization algorithms where activity modifies the relative strength of inputs while conserving total synaptic weights or overall neuronal activity[7]. Although these algorithms do not pretend to biophysical realism, they imply the existence of an intracellular signalling system that would render synapses 'aware' of each other or of mean neuronal activity. Here, we tested whether synaptic normalization is operative when particular inputs to a given neuron are subjected to stimulation protocols producing long-term depression (LTD) and long-term potentiation (LTP). For methodological reasons that will become clear below, these experiments were performed in intercalated (ITC) neurons of the amygdala[8]. ITC cells are spiny GABA (γ-aminobutyric acid) neurons located between the basolateral amygdala (BLA) and the central nucleus (Fig. 1A, grey ovals). They receive topographically organized glutamatergic inputs from the BLA.

To activate different groups of BLA axons converging on single ITC cells, an array of closely spaced (~150 μm) stimulating electrodes (Fig. 1A, black dots) was positioned in the BLA. Below, stimulation sites are given arbitrary numbers that increase as their position shifts lateromedially. To assess the selectivity of this stimulation method, we tested whether responses evoked in ITC cells ($n = 9$) from different BLA sites occluded each other. Stimuli were delivered at each BLA site independently (Fig. 1Ba, top) or two at a time (Fig. 1Ba, bottom). The amplitude of excitatory postsynaptic currents (EPSCs) evoked by paired stimuli, normalized to that observed following summation of responses evoked by single stimuli, was plotted as a function of the interval between paired stimulation sites (Fig. 1Bb). Response occlusion was seen only with neighbouring sites (paired t-test, $P < 0.05$), suggesting that this stimulation method was relatively selective.

The BLA sites that evoked the largest responses were always located at the same mediolateral level as the recorded soma. This suggested that there is a correspondence between the mediolateral

